CHEMICAL ENGINEERING TRANSACTIONS
VOL. 81, 2020
A publication of AIDIC
The Italian Association of Chemical Engineering
Online at www.cetjournal.it
Guest Editors: Petar S. Varbanov, Qiuwang Wang, Min Zeng, Panos Seferlis, Ting Ma, Jiří J. Klemeš

ISBN 978-88-95608-79-2; **ISSN** 2283-9216
DOI: 10.3303/CET2081021

Impingement Cooling with Dual Synthetic Jet Based on Improvement of Exit Configuration

Zhiyong Liu, Zhenbing Luo*, Zhijie Zhao, Xiong Deng, Tianxiang Gao

College of Aerospace Science and Engineering, National University of Defense Technology, Changsha, China
luozhenbing@163.com

The effect of impingement cooling using a dual synthetic jet actuator (SJA) with improvement of exit configuration has been investigated experimentally. A hump with cross section of a half-elliptic shape was attached to the flat between the two exits of the SJA. Due to Coanda effect, spread of the synthetic jet was enhanced. Two different humps with height to half width ratios of e = 1.0 and 1.5 have been tested. An infrared camera was utilised to record the temperature of the cooled plate. Statistical results of the temperature have been discussed. With humps, average temperature of the impinged area decreased about 2.6 °C and 0.6 °C corresponding to e = 1.0 and 1.5. Standard deviation of the temperature in the impinged area was almost unchanged. Effective cooled area on the plate was enlarged significantly. For e = 1.0 and 1.5, the effective cooled area with temperature below 20 °C increased by 1.1 and 0.5 times. It means that the improvement is very helpful to applications of electrothermal cooling that involve large cooled area.

1. Introduction

Enhancement of heat transfer is very common in industry, for example in electronics. As electronic components develop with decreasing volumes, their power densities increase. High efficient techniques of heat transfer are active demand. Impingement cooling by jets is thought to be an effective heat transfer technique (Pavlova & Amitay 2006). Considering the availability, lower cost and convenience, gas is usually chosen as working fluid. Large amount of investigations on impingement cooling with gas jets have been conducted. He et al. (2015) compared the enhancement effects of steady jet and synthetic jet and reported that synthetic jet had higher efficiency of heat transfer. Experimental investigation performed by Tan et al. (2015) also confirmed the effect. Synthetic jet is characterized by zero-net mass flux and has the advantages of no plumbing system and small footprint area. These features make synthetic jet a promising technique for cooling electronic components and more adaptable in practical applications.

Synthetic jet is formed by synthesis of a train of vortices emitted from an orifice or a slot. The orifice is an exit of a chamber whose volume is compressed and dilated alternately through a diaphragm. Smith & Glezer (1998) introduced a new type of synthetic jet actuator (SJA) called piezoelectric SJA. It is further compatible with compact design for its miniature volume. Later Glezer and Amitay (2002) reviewed the evolution of a synthetic jet and the flow control mechanism. Mahalingam et al. (2004) utilised SJA to conduct thermal management. Ghaffari et al. (2016) studied the effect of heat transfer by using a slot impinging synthetic jet. Their results indicated that the jet-to-surface spacing was crucial to heat transfer and maximum cooling performance was achieved with dimensionless spacing in the range of 5 ~ 10. This feature was associated with the coherence vortex structures. Gil & Wilk (2020) investigated impingement cooling with SJA in a large scope of geometry and supply parameters and proposed new heat transfer correlations. Researches focused on efficiency of energy utilization (Greco et al. 2018), advanced design of SJA and optimization of operational parameters (Krishan et al. 2019) have also been conducted.

In regard of efficiency of energy utilisation, Luo et al. (2006) proposed a dual synthetic jet actuator (DSJA) which is featured by two chambers with two exits and sharing a diaphragm. When the diaphragm vibrates, one chamber is compressed and gas is ejected with relatively high velocity from the associated exit. The other chamber is dilated and gas is suctioned with relatively low velocity from the other exit. This process alternately

Paper Received: 08/03/2020; Revised: 25/05/2020; Accepted: 01/06/2020
Please cite this article as: Liu Z., Luo Z., Zhao Z., Deng X., Gao T., 2020, Impingement Cooling with Dual Synthetic Jet Based on Improvement of Exit Configuration, Chemical Engineering Transactions, 81, 121-126 DOI:10.3303/CET2081021

occurs and results in a jet at downstream. Since the vibration energy of the diaphragm directly contributes to jet generation in both ejection and suction phases, the efficiency of energy utilisation is almost two times to that of conventional SJA. Deng et al. (2017) combined dual synthetic jet actuator with small-scale heat sink to control the temperature of a high-power LED. Vectoring jet of DSJA is achieved by an adjustable slider (Deng et al. 2015). Cooled area then is expanded by sweeping flows. However, experimental results (Luo et al. 2016) showed that the cooling capability degraded much when vectoring angle of jet was large.
To enlarge cooled area and keep the cooling capability from being degraded much, an improvement of exit configuration of DSJA has been done. A hump with cross section of a half-elliptic shape was attached to the flat between the two exits of DSJA. Due to Coanda effect, spread of jet was enhanced and larger cooled area has been achieved. Temperature of the impinged plate was measured and some discussion about its statistical results have been done.

2. Experimental approach

2.1 The DSJA and humps

As mentioned above, DSJA looks like that two conventional SJAs are closely abreast (see Figure 1). So the behaviors of the two exits have a phase difference of π. The shared diaphragm is driven by two piezoelectric disks. Geometry parameters, such as length, width and depth of the slots and chambers, are chosen carefully. It follows the principle that the natural resonant frequency of the diaphragm is as close as possible to the Helmholtz frequency of a single chamber. Investigations indicated that excitation with this frequency could obtain the largest exit velocity (Buren et al. 2016). There is a unique geometry parameter that is the distance of the two exits. Previous study (Liu et al. 2019) showed that appropriate distance could avoid self-support phenomenon and result in a strong jet. In present work, the two slot exits of 2 × 20 mm are spaced by 5 mm.

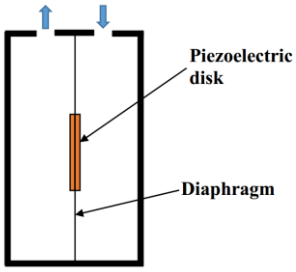

Figure 1: Schematic of DSJA

A hump is attached to the flat between the two slots to improve the synthesis of flows ejected from the two exits (see Figure 2). The cross section of the hump is half-elliptic shape with height of h, width of d = 5 mm and length of l = 20 mm. Due to Coanda effect, gas ejected from one slot attaches to the associated side of the hump. Deflection of flow occurs and spread of the synthetic jet is enhanced. Two humps with different e defined as Eq(1) have been tested.

$$e=\frac{h}{d/2} \tag{1}$$

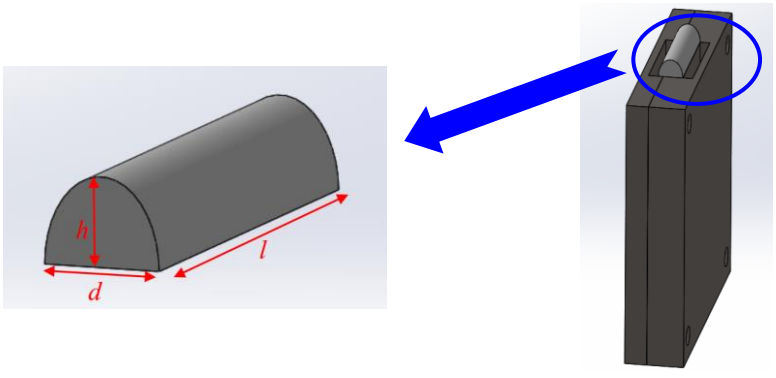

Figure 2: DSJA with a hump

2.2 Experimental setup

A thin steel plate heated by electricity was chosen as the cooled plate. An infrared camera was deployed on one side of the plate to measure its temperature. On the other side, the DSJA was set up to cool the steel plate. Figure 3 shows the schematic of the experimental setup. Since the steel plate is only 0.08 mm, it is assumed that no gradient of temperature exists between the two sides of the plate. In order to improve the accuracy of temperature measurement, the plate was coated with a very thin black paint which has a high emissivity of 0.95.

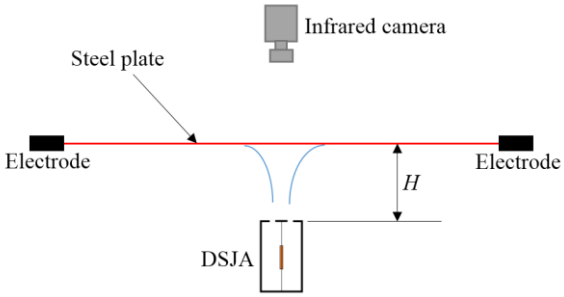

Figure 3: Schematic of the experimental setup

The infrared camera has a resolution of 320 × 240 pixels. Any variation of temperature that is bigger than 0.05 °C can be detected. Infrared thermal images were recorded at 10 Hz with 256 color levels. A room thermometer was used to record the environmental temperature which was also the temperature of the cooling gas. The axis of the slots of the DSJA was vertical to the plate with a distance of *H*. The DSJA was excited by a sinusoidal signal with frequency of 528 Hz and amplitude of 150 V. A maximum velocity of 28 m/s at the slots was achieved. The process of measurement is as follows. Firstly, the plate is heated by electricity with constant power. Its temperature then increases to a certain value at which thermal balance is achieved. After a moment, the DSJA is started and temperature of the plate decreases. Another thermal balance will be achieved and distribution of the temperature of the plate won't vary anymore. This state is kept for a while before the measurement is finished.

2.3 Data reduction

Infrared thermal images are transferred to a computer and analyzed by a specialized software. A rectangular region of 90 × 130 pixels corresponding to 51.4 × 81.3 mm is chosen as the impinged area. Figure 4 shows typical thermal images of the two thermal balance states. Histories of maximum, average and minimum temperatures in the rectangular region are presented in Figure 5.

Analysis of the average temperature in the rectangular region is conducted with the use of classical thermal balance method. For the first balance state, heat loss is attributed to heat transfers of radiation, free convection and conduction. For the descent process and the second balance state, heat transfer of forced convection is involved. The four items related to heat loss are calculated by Eq(2) ~ Eq(5) with Kelwin temperatures. The associated parameters are assigned as these: $\varepsilon = 0.95$, $\sigma = 5.67 \times 10^{-8}$ W/ (m^2*K^4), $A_1 = 51.4 \times 81.3$ $mm^2 = 4.2 \times 10^{-3}$ m^2 and $A_2 = (51.4 + 81.3) \times 2 \times 0.08$ $mm^2 = 2.1 \times 10^{-5}$ m^2.

$$q_{rad}=\varepsilon\sigma A_1(T^4-T_{gas}^4) \tag{2}$$

$$q_{fc}=k_{fc}A_1(T-T_{gas}) \tag{3}$$

$$q_{cond}=-k_{cond}A_2\frac{dT}{dl} \tag{4}$$

$$q_{fdc}=k_{fdc}A_1(T-T_{gas}) \tag{5}$$

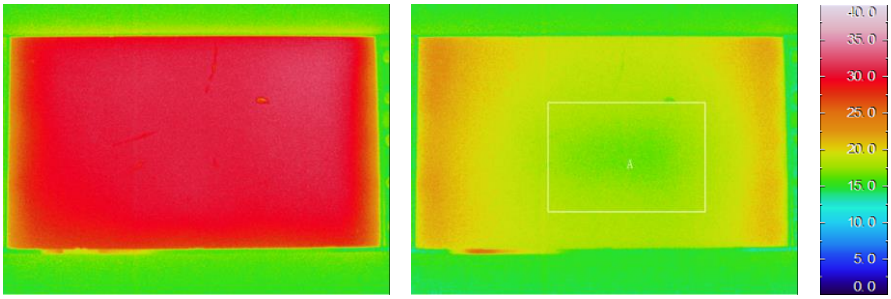

Figure 4: Typical thermal images. Left: at the first balance state; right: at the second balance state.

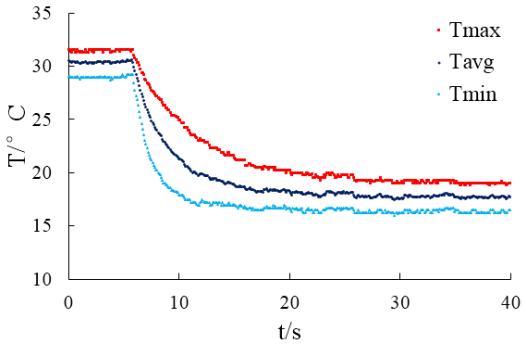

Figure 5: Histories of temperatures

Based on the distribution of temperature of the plate, conductive loss can be calculated and is less than 4 % of the total heat loss. So this item is omitted in next analysis. Considering that there are two sides of the plate, the thermodynamics equations are built as follows.

$$Q_{elec}-2q_{rad}-2q_{fc}=0 \tag{6}$$

$$Q_{elec}-2q_{rad}-q_{fc}-q_{fdc}=Cm\frac{dT}{dt} \tag{7}$$

$$Q_{elec}-2q_{rad}-q_{fc}-q_{fdc}=0 \tag{8}$$

Here Q_{elec} is the heating power of electricity, C is specific heat and m is mass. Eq(6) and Eq(8) describe the first and second thermal balance states. Eq(7) describes the descent process of the temperature. Integrating Eq(7), one can obtain the temperature with following form.

$$T=c_1e^{c_2t}+c_0 \tag{9}$$

Here c_0, c_1 and c_2 are constants. Figure 6 shows the comparison of calculated and measured temperatures. It is seen that the agreement is very good. This validates the analysis of thermodynamics.

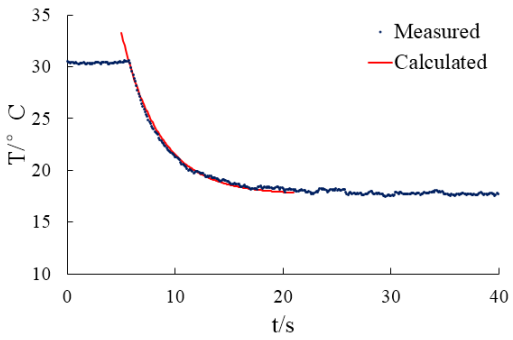

Figure 6: Comparison of temperatures

Combining Eq(6) and Eq(8), the forced convection coefficient k_{fdc} can be determined (see Eq(10)). T_2 corresponds to the average temperature at the second balance state. The k_{fdc} is the exact parameter that is used to evaluate the cooling effect of DSJA.

$$k_{fdc}=\frac{Q_{elec}-2q_{rad}(T_2)}{A_1(T_2-T_{gas})}-k_{fc} \tag{10}$$

3. Results and discussion

Two humps of e = 1.0 and 1.5 have been tested. The DSJA was deployed at d = 9.2 which is defined by Eq(11). The second thermal balance state was checked. Average temperature and standard deviation of temperature in the rectangular area are displayed separately in Figure 7. For comparison, values of cases with no hump are plotted at e = 0. It can be seen that cooling effect is enhanced by the humps. About 2.6 °C reduction has been achieved with e = 1.0, 0.6 °C was dropped with e = 1.5. However, the standard deviation of temperature seems to be unchanged nearly.

$$d=\frac{H}{2\sqrt{S_{slot}/\pi}} \tag{11}$$

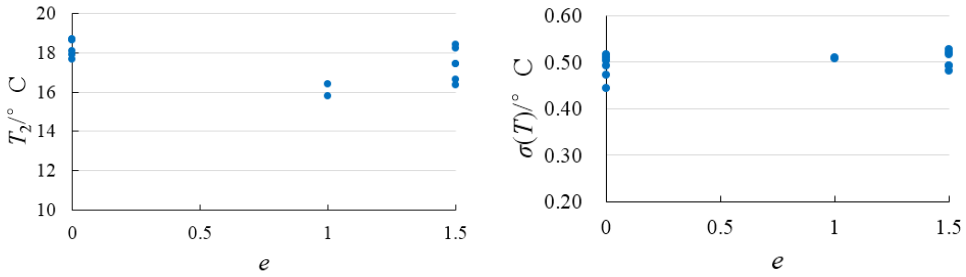

Figure 7: Temperatures with humps. Left: average temperature; right: standard deviation.

Cooling capability is judged directly by the forced convection coefficients. Figure 8 shows the k_{fdc} which is calculated by Eq(10) and corresponds to the rectangular region. It is seen that k_{fdc} is enlarged significantly. Approximate 100 % and 30 % increment of k_{fdc} are obtained with e = 1.0 and 1.5. Due to the insufficiency of data at e = 1.0, the enhancement of cooling effect may be overestimated.

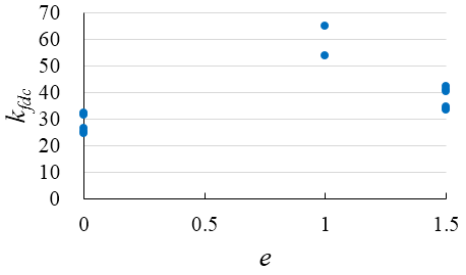

Figure 8: Forced convection coefficients

The cooling effect on the plate can also be evaluated by effective cooled area at the second thermal balance state. Effective cooled area is the area with temperature less than a specified temperature. Ratios of the effective cooled area to the plate's total area are plotted in Figure 9. Though the scatter of data is a little wide, the trend of improvement is obvious. The largest effective cooled area is achieved with e = 1.0. For the specified temperature of 20 °C, the effective cooled area increases by 1.1 and 0.5 times with e = 1.0 and 1.5there. The effective cooled area reduces rapidly as the specified temperature decreases. However this doesn't happen to the cases of e = 1.0. These behaviors are consistent with the variations of average temperature in the rectangular region. To some degree, the consistency indicates that choosing the rectangular region as the impinged area is reasonable.

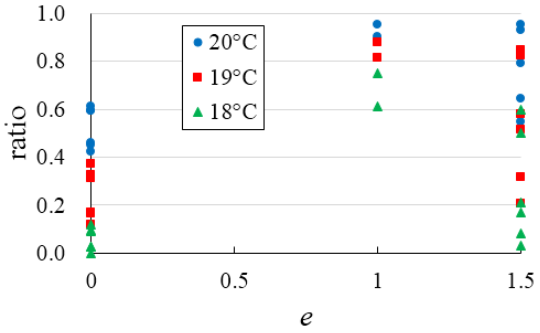

Figure 9: Ratios with different specified temperatures

4. Conclusions

Investigation of impingement cooling with improvement of exit configuration of DSJA has been conducted. Results show that the cooling capability of DSJA is enhanced significantly. In the impinged area, 2.6 °C reduction has been achieved with hump of e = 1.0, accompanied by a large effective cooling area. In future, this effect will be examined with higher heating power to check the cooling potential of DSJA.

Acknowledgements

The authors gratefully acknowledge the financial supports for this work from the National Natural Science Foundation of China (grant Nos. 11872374 & 11602299).

References

Buren T.V., Whalen E., Amitay M., 2016, Achieving a high-speed and momentum synthetic jet actuator, Journal of Aerospace Engineering, 29(2), 04015040.

Deng X., Xia Z.X., Luo Z.B., Li Y.J., 2015, Vector-adjusting characteristic of dual-synthetic-jet actuator, AIAA Journal, 53(3), 794-797.

Deng X., Luo Z.B., Xia Z.X., Gong W.J., Wang L., 2017, Active-passive combined and closed-loop control for the thermal management of high-power LED based on a dual synthetic jet actuator, Energy Conversion and Management, 132, 207-212.

Ghaffari O., Solovitz S.A., Arik M., 2016, An investigation into flow and heat transfer for a slot impinging synthetic jet, International Journal of Heat & Mass Transfer, 100, 634-645.

Gil P., Wilk J., 2020, Heat transfer coefficients during the impingement cooling with the use of synthetic jet, International Journal of Thermal Sciences, 147, 106132.

Glezer A., Amitay M., 2002, Synthetic jets, Annual Review of Fluid Mechanics, 34, 503-529.

Greco C.S., Paolillo G., Ianiro A., Cardone G., Luca L., 2018, Effects of the stroke length and nozzle-to-plate distance on synthetic jet impingement heat transfer, International Journal of Heat & Mass Transfer, 117, 1019-1031.

He X., Lustbader J.A., Arik M., Sharma R., 2015, Heat transfer characteristics of impinging steady and synthetic jets over vertical flat surface, International Journal of Heat & Mass Transfer, 80, 825-834.

Krishan G., Aw K.C., Sharma R.N., 2019, Synthetic jet impingement heat transfer enhancement – A review, Applied Thermal Engineering, 149, 1305-1323.

Liu Z.Y., Luo Z.B., Liu Q., Deng X., Peng W.Q., 2019, Self-support phenomenon and formation characteristics of dual synthetic jet, Sensors and Actuators A, 299, 111597.

Luo Z.B., Xia Z.X., Liu B., 2006, New generation of synthetic jet actuators, AIAA Journal, 44 (10), 2418-2419.

Luo Z.B., Deng X., Xia Z.X., Wang L., Gong W.J., 2016, Flow field and heat transfer characteristics of impingement based on a vectoring dual synthetic jet actuator, International Journal of Heat & Mass Transfer, 102, 18-25.

Mahalingam R., Rumigny N., Glezer A., 2004, Thermal management using synthetic jet ejectors, IEEE Transactions on Components & Packaging Technologies, 27, 439-444.

Pavlova A., Amitay M., 2006, Electronic cooling using synthetic jet impingement, Journal of Heat Transfer, 128, 897.

Smith B. L., Glezer A., 1998, The formation and evolution of synthetic jets, Physics of Fluids, 10, 2281-2297.

Tan X.M., Zhang J.Z., Yong S., Xie G.N., 2015, An experimental investigation on comparison of synthetic and continuous jets impingement heat transfer, International Journal of Heat & Mass Transfer, 90, 227-238.